Scintillator Phosphors for Medical Imaging

Enabling life-saving diagnostics

by Steven J. Duclos

Scintillators are high density luminescent materials that convert X-rays to visible light. These materials have been used since the turn of the century to dramatically enhance the sensitivity of film cartridges used in medical diagnostics. Coupling scintillators to photodiodes, charge coupled devices (CCDs), and photomultiplier tubes (PMTs) is an efficient way to convert X-rays to electrical signals. This has ushered in an era of diagnostic imaging which requires advanced scintillators with enhanced properties, such as increased X-ray conversion efficiency, faster luminescence decay times, lower afterglow, and greater stability in the radiation field. In addition to medical diagnostics, scintillators are used in X-ray security apparatus, industrial inspection, and in high-energy physics calorimetry. Therefore, the field of scintillator materials is quite extensive, and for more complete discussions the reader is directed to reviews by Weber (1), Blasse, et al. (2), and Lempicki, et al. (3).

The present review is restricted to inorganic scintillator materials that are currently used in the field of medical

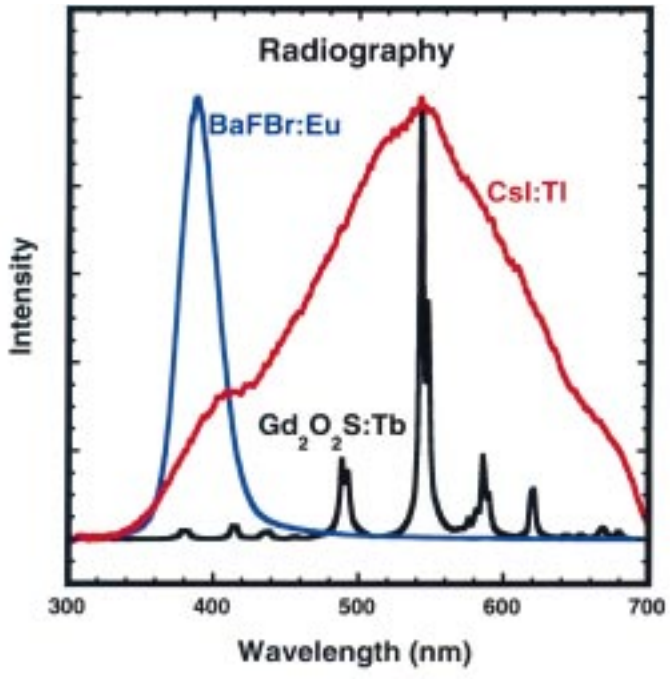

FIG. 1. Room temperature luminescent spectra for scintillators used for radiography. These are the spectra excited by 60 kVp X-rays. The spectra have been normalized to their peak output. Although the storage phosphor BaFBr:Eu is not measured when directly excited by X-rays, its output spectrum is essentially the same when a readout laser is used to excite the stored energy.

Table 1: Scintillators used in mediccal X-ray detection and their properties.

Name	Formula	Medical Application	Density (g/cm^3)	Speed (s)	Emission Peak (nm)	Relative Light Output
Gadolinium Oxysulfide	Gd_2O_2S:Tb	Radiology	7.34	$3x10^{-3}$	540	
Barium Fluorobromide	BaFBr:Eu	Radiology	5.20	$800x10^{-9}$	390	-
Cesium Iodide	CsI:Tl	Radiology	4.51	$980x10^{-9}$	550	100
Cadmium Tungstate	$CdWO_4$	Computed Tomography	7.99	$14x10^{-6}$	480	30
Yttrium-Gadolinium Oxide	$(Y,Gd)_2O_3$:Eu	Computed Tomography	5.95	$1x10^{-3}$	611	70
Gadolinium Oxysulfide	Gd_2O_2S:Pr	Computed Tomography	7.34	$3x10^{-6}$	513	75
Sodium Iodide	NaI:Tl	Nuclear cameras	3.67	$230x10^{-9}$	415	70
Bismuth Germanate	$Bi_4Ge_3O_{12}$	PET	7.13	$300x10^{-9}$	480	15
Gadolinium Orthosilicate	Gd_2SiO_5:Ce	PET	6.71	$40x10^{-9}$	430	20

imaging. Despite this restriction we will encounter a variety of oxide, oxysulfide, fluoride, and alkali halide materials. Depending on the application the scintillators are in the form of single crystals, polycrystalline ceramics, or powders. Optimization of a scintillator for an application requires an understanding of electron and hole transport, electronic defect creation, luminescence processes, and optical transport in materials. Following a brief discussion of the scintillation process and properties required by scintillators, representative materials will be reviewed by medical imaging modality: (1) radiography, (2) computed tomography (CT), and (3) nuclear cameras and positron emission tomography (PET). TABLE 1 lists the scintillators that will be covered in this review, as well as some of their physical properties.

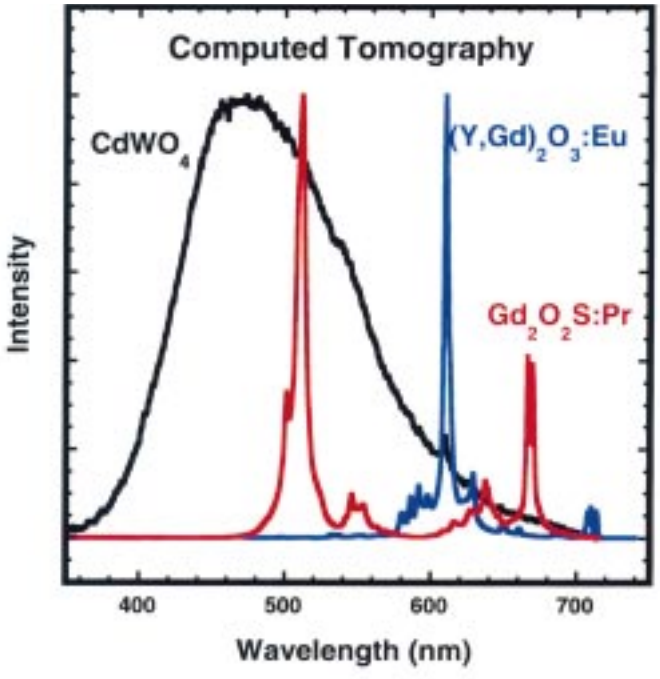

FIG. 2. Room temperature luminescent spectra for scintillators used for computed tomography. These are the spectra excited by 60 kVp X-rays. The spectra have been normalized to their peak output.

The Scintillation Process and Its Relation to Materials Properties

The generation of visible photons from X-rays is a three step process. The X-ray must first be stopped and its energy dissipated into the material. Depending on the energy of the X-ray, $E_{x\text{-}ray}$, its dissipation results from the photoelectric effect, Compton scattering, or pair production. In each case the energy is ultimately dissipated into phonons and mobile electrons and holes. When these free electrons and holes have given up sufficient energy to the lattice they can pair to form excitons. While the theoretical limit of the number of excitons created is $n'_{e\text{-}h} = E_{x\text{-}ray}/E_{gap}$, where E_{gap} is the scintillator band gap, the measured exciton number (4) is $n_{e\text{-}h} = n'_{e\text{-}h}/\beta$, where β is typically greater than 2. It is the excitons that release their energy to the luminescent centers, so the scintillation efficiency will be optimized for materials with smaller βs and lower E_{gap}. The role of electrons in the X-ray stopping process clearly indicates that those materials with higher electron densities will stop X-rays in shorter distances. Therefore scintillator materials typically employ heavy elements, and have densities greater than 5 g/cm^3.

The second step in the scintillation process is the capture of the exciton energy by the luminescent center or activator. As in lighting phosphors, such centers can be intrinsic to the host lattice or can be ions deliberately doped into the lattice. Not every exciton results in an excited luminescent center since electronic defects also trap electrons and holes, and often result in release of this energy through non-radiative processes. Such defect trapping can result in color centers and optical absorption at the luminescent wavelength, which results in radiation induced damage to the scintillator efficiency. If the defect trap is shallow, thermal processes can result in the delayed regeneration of a free electron or hole followed by excitation of the luminescent center. Such delayed emission is referred to as afterglow, and can be quite deleterious to a scintillator in certain applications. On the other hand, storage phosphors used in radiography depend on the efficient trapping and storage of these charges. This second step in the scintillation process is the subject of most scintillator materials engineering. The control of trapping defects through processing and secondary doping can have a profound effect on critical properties of a scintillator.

The third step is the radiative emission of a photon from the luminescent center. The total probability of a transition occurring from an excited state to the ground state is the sum of the probability of the radiative emission of a photon, A_r, and a non-radiative probability, A_{nr}. The competition between A_r and A_{nr} is a complex function of the strength and symmetry of the crystal field around the luminescent center, the host phonon spectrum, the transition energy, and that energy's proximity to other energy levels in the material. The probability A_r will be largest when the initial and final states are of opposite parity and the same total spin (5). Theoretically, the radiative probability is otherwise zero, however, mixing of higher energy states into the excited state generally results in a finite radiative transition probability. The decay rate of the scintillator once the X-ray excitation has been turned off is determined by $e^{-t/\tau}$, where $\tau = 1/A_r$. For medical applications such as PET, which involve the counting of individual X-ray photons, the counting rate and signal can be limited by the scintillator speed. Processes that increase A_{nr} result in lower quantum efficiency of the luminescent center and lower scintillation efficiency. Non-radiative processes include the energy relaxation via the emission of phonons and transfer of the excited state energy to other centers nearby, including impurities.

The three steps outlined above determine the emission efficiency of the scintillator material. There are other important materials aspects that determine the efficiency of the scintillator when it is incorporated into an X-ray detection system. For example, the particle size of a scintillator screen used in conjunction with film will affect the light scattering properties and, if not optimized, can degrade the spatial resolution of the device. For crystalline scintillators the light output can be affected by the efficiency of light reflection and refraction at interfaces. A scin

(continued on next page)

tillation photon, which is emitted from the luminescent center isotropically, can undergo many interactions with the scintillator wall before encountering the crystal face coupled to the photodiode. Optical transparency is especially important in geometries where the photon path length is long. Internal scattering will increase the path length and make the material more sensitive to radiation induced optical absorption. For example, scintillator transparency and efficient wall reflectivity is critical to detector pixels used in computed tomography where spatial resolution and protection of the photodiode from direct hits by transmitted X-rays requires a high thickness to width aspect ratio.

Radiography

Radiography refers to the technique where the patient is placed between an X-ray source and an X-ray detector, typically a film cartridge. Anatomic features, such as bones and tumors, differ in X-ray absorption from their surroundings and their shadows are projected onto the detector. X-ray film itself is not sufficiently dense to stop the 30-100 keV X-rays used, so scintillator screens are typically employed to increase the stopping power. The film then registers the light from the scintillator rather than the X-rays themselves. More recently film has been replaced with electronic systems which also depend on scintillators for efficient capture of the transmitted X-rays. One device is the storage screen which, after exposure to X-rays, is read out with a laser system and digitized. The scintillation process is critical to all of these devices and the materials used will be described below.

The sensitivity and X-ray capture of a film screen is enhanced by sandwiching the film between layers of a powdered scintillator, typically gadolinium oxysulfide doped with terbium as an activator, Gd_2O_2S:Tb (6). The emission spectrum of Gd_2O_2S:Tb under X-ray excitation is shown in FIG. 1. It has a strong peak at 540 nm due to the $^5D_4 \rightarrow {}^7F_J$ transitions within the *f* manifold of the Tb ion. This wavelength is well matched to green sensitive medical film. The morphology and size of the particles in the scintillator film is critical to avoid excessive light scattering which degrades the resolution of the system (7). The thickness of the scintillator layer must also be carefully controlled, and it is designed to balance the added stopping power of a thicker layer with the resulting loss of spatial resolution due to light scattering. Synthesis techniques are used that minimize the creation of electronic defects since excessive afterglow will result in a ghost image of one patient onto the film of the next patient, which is a situation that must be avoided.

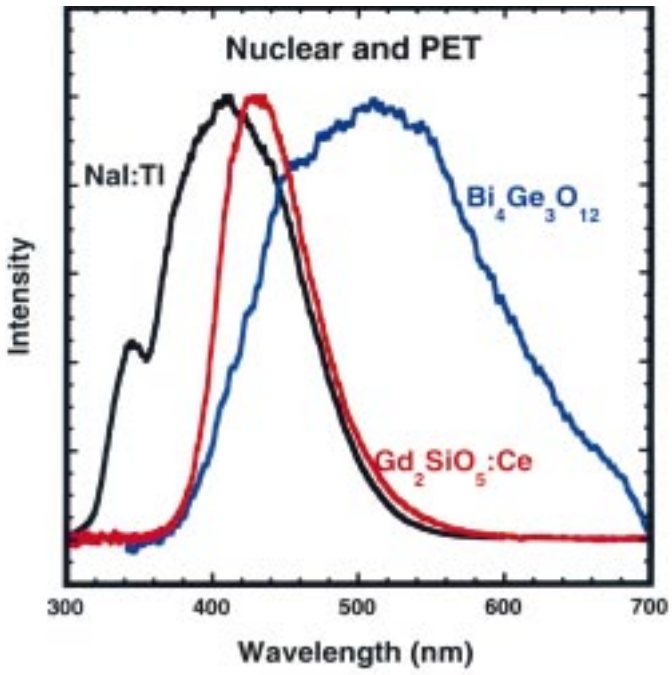

FIG. 3. Room temperature luminescent spectra for scintillators used for nuclear cameras and PET. These are the spectra excited by 60 kVp X-rays. The spectra have been normalized to their peak output.

In 1983, the storage phosphor BaFBr:Eu was introduced (8) which stores the X-ray energy in electronic defects. These defects are emptied at a later time by scanning with a laser which releases energy to the Eu^{2+} activator. The Eu^{2+} blue emission (FIG. 1) is proportional to the X-ray flux stored on the panel and is detected with a blue sensitive photomultiplier tube (PMT). An image is generated by recording the PMT output versus the position of the excitation laser. The scintillator has a density of 5.20 g/cm^3, and the Eu^{2+} excited state has a lifetime of 800 nsec, which determines the rate at which the panel can be read by the laser. Considerable effort has gone into determining and optimizing the defect responsible for the energy storage (9, 10).

Cesium iodide activated with thallium, CsI:Tl, is used as a scintillator in image intensifiers. A thin film of CsI:Tl is placed in front of a photocathode which generates electrons from the scintillation light. These electrons are then electrostatically amplified and converted back to light by a cathodoluminescent material for viewing of the image. These images can also be captured on CCDs, generating digital data which can be transmitted and analyzed remotely. CsI:Tl has a broad emission (see FIG. 1) from 350 nm to 700 nm with a peak at 550 nm. The emission is from parity allowed ($sp \rightarrow s^2$) transitions $^3P_1 \rightarrow {}^1S_0$ and has a lifetime of 980 nsec, which is fast enough to allow these devices to be used for fluoroscopy. The allowed nature of this transition contributes to its high light output. Its application in image intensifiers is aided by the blue component of its scintillation light, which is particularly efficient in generating electrons in the photocathode. Undoped CsI also luminesces from states that trap the free excitons generated by X-rays. These self-trapped excitons recombine and release that energy radiatively. However, CsI without doping has considerably lower light output due to competition by non-radiative defects for the exciton energy.

Computed Tomography

Computed tomography (CT) measures the attenuation of X-rays through the body as an X-ray source and opposed detector rotate 360° in a plane around the patient. Images of internal organs are generated by back projecting detector readings at the collected angles. Typically fan beam X-ray sources and arc detectors are employed to increase the information gathered and improve image quality. The scintil-

lators used in CT must be capable of measuring attenuation differences of 1 part in 1000, show little afterglow, and be stable in the radiation field over the time of an extended scan (typically 60 seconds). For example, afterglow will result in an image artifact if a dense object (such as a bone) rapidly eclipses the X-ray intensity and the signal in the detector is dominated by the scintillator afterglow rather than the X-ray photons passing through the anatomy and striking the detector. Three scintillators currently used in CT machines will be reviewed here: cadmium tungstate, a single crystal scintillator with intrinsic emissions, and two ceramic scintillators, yttria-gadolinia oxide activated by Eu, and gadolinium oxysulfide activated by Pr.

Cadmium tungstate, $CdWO_4$, is a colorless oxide single crystal which is grown at 1240°C by Czochralski techniques (11). Its density is 7.99 g/cm^3 and has a broad emission between 400 and 600 nm peaking at 480 nm (FIG. 2). The light output is adequate for CT scanners, and its afterglow is among the lowest of the materials used in these detectors. The emission originates from the WO_4 tetrahedra in this monoclinic structure material. $CdWO_4$ exhibits a cleavage plane along the (010) crystallographic plane which is so weak that the material can be cut with a razor blade. Chipping and cracking during dicing into pixels can result in undesirable pixel-to-pixel nonuniformities in light collection efficiency.

Defects generated in the material upon exposure to X-rays result in absorption into the visible region and self-absorption of the scintillation emission. Therefore, $CdWO_4$ has a radiation damage which must be compensated for during image reconstruction. Recent developments in the growth techniques of $CdWO_4$ have reduced this radiation damage susceptibility. These include the minimization of impurity defects and reduction of Cd vacancy defects by replacement of the CdO evaporated during high temperature growth (11). Extensive doping of the crystal to improve properties such as radiation damage have not been accomplished, most likely due to difficulties in uniformly doping the single crystals.

Solid solutions of yttria and gadolinia with Eu as an activator, $(Y,Gd)_2O_3$:Eu, represent a dense version of the high quantum efficiency Y_2O_3:Eu red phosphor. Its melting temperature of 2439°C makes single crystal growth difficult, so these materials are prepared as polycrystalline ceramics that are sintered to transparency (12). The structure of $(Y_xGd_{(1-x)})_2O_3$ is cubic at its preparation temperatures for $x < 0.4$. The isotropic optical properties of the cubic structure allows for sintering to complete transparency. The emission of the Eu is from 550 nm to 720 nm (FIG. 2) with a strong peak at 611 nm, which is well suited to detection by photodiodes. The lifetime of this state is slightly less than 1 ms. At $x = 0.3$ the material density is 5.95 g/cm^3, sufficient to stop 99.96% of 70 keV X-rays in 3 mm.

The ceramic process allows for the homogeneous doping of additives, in addition to the activator, which are useful for the control of critical scintillation properties (13). Similar to the well known process of doping semiconductors to control electronic properties, these additives are used to affect the electronic defects and energy migration between them, which are responsible for afterglow and radiation damage. As an example, the addition of either Pr or Tb to the $(Y_xGd_{(1-x)})_2O_3$:Eu scintillator can reduce afterglow by more than an order of magnitude, even at levels of 100 ppm. The Eu activator is a strong electron trap which can leave holes available for trapping at defect sites. The addition of Pr or Tb, which are strong hole traps, competes for holes with the afterglow trap and decay non-radiatively when associated with a nearby Eu ion. Although this process also decreases the efficiency of the scintillator, the high intrinsic efficiency of this material allows for this tradeoff (14). Uniformity of scintillation properties demands that such potent additives be uniformly mixed into the lattice, which is accomplished in the ceramic process by coprecipitating the additives along with the host ions.

A second ceramic now being used as a scintillator in CT scanners is gadolinium oxysulfide activated with Pr (15), Gd_2O_2S:Pr. This material has a predominant emission at 513 nm (FIG. 2), which results from the $^3P_0 \rightarrow {}^3H_J, {}^3F_J$ transitions within the Pr ion, which is nominally doped to 1%. This transition is spin-allowed (although it still is an *f-f* configuration transition so is parity disallowed), which makes it reasonably fast with a decay time of 3 μs. The structure of this material is hexagonal, which results in decreased light transmission due to scattering at index mismatches at the randomly-oriented grain boundaries. Hot isostatic pressing (HIP) is used to improve the transparency (16), and doping has been used to improve the scintillation properties. Ce is added at approximately 100 ppm for afterglow reduction. Li_2GeF_6 is used as a HIP aid, which improves the bulk transparency and scintillator light output (16).

Nuclear Cameras and PET

Nuclear cameras and positron emission tomography (PET) both work by detecting high energy gamma rays emitted from a patient that has ingested short-lived radio-pharmaceuticals. Detecting the spatial distribution of these pharmaceuticals yields information on biological activity in the organs of interest, although the spatial resolution of these cameras is less than for CT. In nuclear cameras a large area detector is comprised of scintillator segments coupled to PMTs. Interpolation of the PMT outputs determines the position that the gamma ray intercepted the camera. Energy resolution is used to eliminate those gamma rays that have been scattered into the detector. Linearity of the scintillator signal with X-ray energy is critical for proper discrimination between scattered and direct gamma rays. In PET the radio-pharmaceutical generates positrons which are rapidly annihilated, generating two 512 keV gamma rays emitted in opposite directions. A ring of detectors surrounds the patient and timing coincidence is used to detect an annihilation. An image of annihilation events, and therefore density of the radio pharmaceuticals, is generated by summing lines projected between detector elements that detect coincident gamma rays. For scintillators used in PET very fast decay times ($\tau < 300$ ns) and high density ($\rho > 7$ g/cm^3) are critical for proper registration of gamma ray coincidence.

Sodium iodide activated with thallium, NaI:Tl, is used in nuclear cameras, although it has relatively low density of 3.67 g/cm^3. It can be grown in large single crystal boules that makes possible the thick transparent scintillators required for stopping gamma rays. Rapid growth rates of these crystals also results in low cost of manufacture. The emission is a broad band extending from 300 nm to 500 nm, peaking at 415 nm (FIG. 3), which is well matched to blue sensitive PMTs. The decay time of the $^3P_1 \rightarrow {}^1S_0$ transition on the Tl^+ activator is 230 ns which is adequate for X-ray photon counting devices. This material is a popular choice for scintillator applications that are not sensitive to the effects of its radiation damage due to color center formation and its relatively low density. Also, the material is hygroscopic and must be protected from ambient atmosphere. Notice that the emission in NaI:Tl has a considerably shorter wave-

(continued on next page)

length than CsI:Tl which is due to the high sensitivity of the exposed s^2 electrons on the Tl^+ ion to the stronger crystal field of the NaI lattice.

Bismuth germanate, $Bi_4Ge_3O_{12}$, is an intrinsic emission scintillator with a high density of 7.13 g/cm^3 and rapid decay time of 300 ns. Although its scintillation efficiency is considerably lower than NaI:Tl, its energy resolution and linearity are excellent. Its density allows for the absorption of 95% of 512 keV gamma rays in 3 cm thickness, which is ideal for coincidence counting applications such as PET. $Bi_4Ge_3O_{12}$ has a broad band emission (FIG. 3) from 400 nm to 550 nm peaking at 480 nm, which is well coupled to the PMT sensitivity. The material has a relatively low melting temperature (1044°C) for an oxide material, and single crystals are typically grown by the Czochralski method (17).

A third material used in high energy X-ray detection is the family of cerium doped gadolinium and lutetium orthosilicates, $(Gd_xLu_{(1-x)})_2SiO_5$:Ce. These materials make use of the parity allowed $^5d \rightarrow {}^4f$ transitions within the Ce ion. The emission for Gd_2SiO_5:Ce (see FIG. 2) is broad, extending from 380 nm to 500 nm peaking at 430 nm. These transitions are among the fastest in the rare-earth series, with the decay times ranging from 40 to 60 ns in the orthosilicates. The crystal structure of Gd_2SiO_5 is monoclinic which makes the material susceptible to cleavage during dicing. These materials are grown as single crystals using the Czochralski technique, at rates of about 1 mm/h. In the case of Lu_2SiO_5 the segregation coefficient of Ce is 0.2, and care must be taken to adjust the melt composition during growth to compensate for the increasing Ce concentration (18). Homogeneous doping is important to ensure linearity of light output with X-ray energy. For example, a lower concentration of activator on the front volume of the crystal, where lower energy X-rays are preferentially captured, would result in a lower than expected light output for these X-rays.

Summary

We have covered here a few of the scintillator materials used in the medical field. The list is not exhaustive, and advancements in the understanding of luminescence physics and material processing is expected to result in scintillators with improved properties. These advances will also be driven by other scintillator uses, not discussed here, such as industrial X-ray inspection, airport and postal security, oil well logging, and high energy physics experimentation. As pointed out throughout this review, no ideal scintillator exists that has the properties required by all applications, and it is expected that specialized scintillator materials will continued to be optimized for specific applications. ■

About the Author

Dr. Steven J. Duclos is is a physicist in the Ceramic Laboratory of the General Electric Corporate Research and Development Center in Schenectady, New York. His current work focuses on improvements in the properties of the ceramic scintillator used in General Electric's Computed Tomography imaging machines.

References

1. M. J. Weber, *Calorim. High Energy Phys., Proc. 5th Int. Conf.*, H. A. Gordon and D. Rueger, eds., World Scientific: Singapore, p. 17 (1995).
2. G. Blasse and B. C. Grabmaier, *Luminescent Materials* (Springer-Verlag, New York 1994).
3. A. Lempicki, A. J. Wojtowicz, and C. Brecher, *Wide-Gap Luminescent Materials*, Stanley R. Rotman, ed., Kluwer Academic Publishers, Boston, p. 235 (1997).
4. P. A. Rodnyi, P. Dorenbos, and C. W. E. Van Eijk, *Scintillator and Phosphor Materials*, M. J. Weber, P. Lecoq, R. C. Ruchti, C. Woody, W. M. Yen, R. Zhu, Eds., Materials Research Society Symposium Proceedings **348**, p. 379 (1994).
5. G. F. Imbusch, *Luminescence Spectroscopy*, M. D. Lumb, ed., Academic, p. 1 (1978).
6. K. A. Wickersheim, R. V. Alves, and R. A. Buchanan, *IEEE Trans. Nucl. Sci.* **17**, 57 (1970).
7. J. D. Kingsley, *Real-Time Radiologic Imaging: Medical and Industrial Applications*, ASTM STP 716, D. A. Garrett and D. A. Bracher, Eds., American Society for Testing and Materials, p. 98 (1980).
8. N. Kotera, S. Eguchi, J. Miyahara, S. Matsumoto, H. Kato, United States Patent No. 4,239,968 (1980).
9. H. H. Ruter, H. von Seggern, R. Reiniger, and V. Saile, *Phys. Rev. Lett.*, **65**, 2438 (1990).
10. F. K. Koschnick, J. M. Spaeth, R. S. Eachus, W. G. McDugle, R. H. D. Nuttal, *Phys. Rev. Lett.*, **67**, 3571 (1991).
11. D. S. Robertson, I. M. Young, and J. R. Telfer, *J. Mat. Sci.*, **14**, 2967 (1979).
12. C. Greskovich, D. A. Cusano, R. J. Riedner, and D. Hoffman, *Am. Ceram. Soc. Bull.*, **71**, 1120 (1992).
13. Greskovich and S. Duclos, *Annu. Rev. Mater. Sci.*, **27**, 69 (1997).
14. R. J. Riedner, R. J. Lyon, D. A. Cusano, C. D. Greskovich, United States Patent No 5,521,387.
15. H. Yamada, A. Suzuki, Y. Uchida, M. Yoshida, H. Yamamoto, and Y. Tsukuda, *J. Electrochem. Soc.*, **136**, 2713 (1989).
16. Y. Ito, H. Yamada, M. Yoshida, H. Fujii, G. Toda, H. Takeuchi, and Y. Tsukuda, *Jap. J. Appl. Phys.*, **27**, L1371 (1988)
17. M. J. Weber and R. R. Monchamp, *J. Appl. Phys.*, **44**, 5495 (1973).
18. C. L. Melcher, R. A. Manente, C. A. Peterson, and J. S. Schweitzer, *J. Cryst. Growth*, **128**, 1001 (1993).

The Total Solution for Fuel Cell Test and Development

Electronic Loads with Windows Software

Control:
Current
Voltage
Power
Mass Flow
Temperature

Measure:
Voltage/Time
Current Density
iR Losses
Tafel Data
MEA Resistance
Long Term Performance

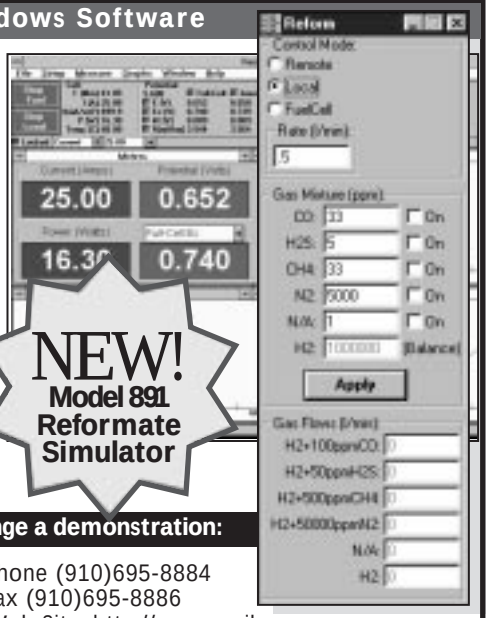

NEW! Model 891 Reformate Simulator

Standard loads from 100 to 5000 watt cell currents of 10 to 500 amperes, other sizes available.
All systems under the control of our FuelCell software for Windows.

Call for more information or to arrange a demonstration:

Scribner Associates, Inc.
150 East Connecticut Ave.
Southern Pines, North Carolina
28387, USA

Phone (910)695-8884
Fax (910)695-8886
Web Site: http://www.scribner.com
E-mail:Sales@Scribner.com

FC198